Fonseca *et al. Herit Sci* (2019) 7:92
https://doi.org/10.1186/s40494-019-0335-1

Heritage Science

RESEARCH ARTICLE Open Access

Seeing red: towards an improved protocol for the identification of madder- and cochineal-based pigments by fiber optics reflectance spectroscopy (FORS)

Beatriz Fonseca[1,2], Catherine Schmidt Patterson[1], Monica Ganio[1], Douglas MacLennan[1] and Karen Trentelman[1*]

Abstract

Fiber optics reflectance spectroscopy (FORS) is commonly used to non-invasively identify madder- and cochineal-based pigments on works of art, but the significant shifts sometimes observed in the position of their diagnostic absorption features can hinder correct interpretation of the spectra. To better understand these shifts, and improve the ability to confidently identify these pigments, a systematic study was carried out to evaluate the effects of different pigment recipes and laking substrates on reflectance spectra. Sixteen different madder- and cochineal-based pigments were synthesized using historical recipes. Each pigment, painted in four different binding media (gum Arabic, linseed oil, beeswax, and egg yolk), was fully characterized by FTIR and HPLC-DAD-MS prior to FORS measurements. The results of the study showed that, in contrast to the absorption features typically used for identification, features in the first derivative transformation of the FORS spectra provided a more robust means of primary identification. In addition, once it has been identified as cochineal, the absorption features in the spectra of cochineal-based pigments could be correlated to the recipe employed, providing a possible means for inferring the method of manufacture and laking substrate from a non-invasive analysis. The results of this study were used to create a decision tree for the identification of madder and cochineal pigments based solely on FORS.

Keywords: Cochineal, Madder, Reflectance spectroscopy, FORS, Absorption, Lake pigments

Introduction

A traditional lake pigment consists of one or more organic dyestuffs adsorbed onto an inorganic substrate (most commonly a type of amorphous hydrated alumina), which renders the colorant insoluble in water and suitable for use as a pigment [1, 2]. In the case of organic red pigments, these are typically extracted from plant sources, such as madder and brazilwood, as well as animal sources, such as kermes, cochineal and lac insects, all of which contain anthraquinone derivatives as colorants [1, 3]. Lake pigments based on madder root have been in use since antiquity [4]. The principal colorants in madder are the dyestuffs alizarin and purpurin (present in different proportions in different species of madder), which have hydroxyl groups attached to the anthraquinone aromatic rings. Lake pigments based on cochineal insects are also commonly encountered in works of art, having been in use in Europe since Medieval times [1, 5]. Armenian, Polish and Mexican cochineal are the main species of insect used for the manufacture of cochineal-based pigments. In all three, the main dyestuff is carminic acid, which, along with hydroxyl and carbonyl groups, also has a glucose unit linked to the anthraquinone core. An important subset of cochineal-based pigments is cochineal carmine, first produced during the seventeenth

*Correspondence: ktrentelman@getty.edu
[1] Getty Conservation Institute, 1200 Getty Center Drive, Suite 700, Los Angeles, CA 90049, USA
Full list of author information is available at the end of the article

century, which consists of carminic acid precipitated in the form of a metal salt or complex (with little to no inorganic substrate) [1, 2, 6].

In the technical analysis of works of art, both madder and cochineal pigments are difficult to accurately identify using non-invasive methods. High performance liquid chromatography (HPLC) has long been employed to identify the specific components of dyes and organic pigments [7–9], and surface enhanced Raman spectroscopy (SERS) [10–13] has also been successfully used to determine the identity of lake pigments. However, both these techniques require the removal of a sample (or addition of a SERS substrate to the analyzed material), which is not always possible. Microspectrofluorimetry [14, 15] provides a non-invasive alternative, but requires the acquisition of both emission and excitation spectra for an accurate identification of the dyestuff. Additionally, microspectrofluorimetry uses high output light, which may not be suitable for the analysis of works of art, and typically lacks portability. By contrast, fiber optics reflectance spectroscopy (FORS), due to its portability and ability to perform non-invasive, in situ analyses, has been increasingly used for the study of organic red pigments in works of art. However, the accurate identification of madder and cochineal lakes by FORS has often been complicated by unwanted spectral contributions of unknown materials present in the paint layer coupled with the variability of the position of characteristic absorption bands, even in seemingly pure samples. Because of these complications, the use of FORS has often been limited to simply classifying unknown organic red pigments as being derived from either plant or animal sources [16–19].

The reflectance spectra of red lake pigments have been widely discussed in the literature [16, 17, 19]. Spectra typically consist of a non-zero reflectance at 350 nm, a local maximum in the blue-green region of the visible spectrum, followed by a steady increase in reflectance around 600 nm which plateaus at the end of the visible region (around 800 nm). A strong absorption band is observed between 350 and 400 nm and is assigned to $\pi \rightarrow \pi^*$ transitions of carbonyl groups in the anthraquinone core [19, 20]. These transitions, which usually occur below 350 nm in the base anthraquinone, are shifted to longer wavelengths in these colorants when electron donor groups, such as hydroxyls, are attached to the anthraquinone aromatic rings [20, 21], as in the case of most organic red dyes. A minor shoulder between 470 and 500 nm is also sometimes visible. Additional absorption features located between 500 and 600 nm are assigned to $n \rightarrow \pi^*$ transitions [19, 20]. In the case of the dyestuffs in madder and cochineal, these features are visible as two absorption sub-bands due to the combination of nonbonding p orbitals of the carbonyl oxygens with delocalized σ wave functions, yielding two weak $n \rightarrow \pi^*$ transitions [22, 23]. Because the mechanism of absorption in anthraquinones is related to electronic transitions between delocalised molecular orbitals, the presence of substituents on the aromatic rings (i.e., functional groups and mordanting ions), their relative positions to each other, as well as the overall chemical environment create electronic and steric effects that affect the position of absorption bands (both below 400 nm and those between 500 and 600 nm) in the resulting spectra [21, 22, 24, 25]. Nevertheless, it is the sub-bands between 500 and 600 nm that are commonly used for identification of organic red pigments [16, 17, 19].

Typical reported values for the two $n \rightarrow \pi^*$ sub-bands in madder pigments are 510–515 nm and 540–545 nm; in cochineal pigments these bands occur between 520–525 nm and 550–565 nm [17, 19, 26, 27]. However, when analyzing works of art, the observed position of these bands can be shifted outside of these ranges, making the identification, or even classification, of an unknown pigment challenging. Along with interferences that may arise from impurities or other pigments present in the paint mixture, differences in the starting material and synthetic pathway result in the formation of pigments with different dyestuff ratios, which can cause visible shifts in the characteristic absorption features used for identification in the reflectance spectrum [1, 4]. This dependence of the reflectance spectrum on the synthetic pathway was highlighted in a study that showed that the position of the aforementioned characteristic $n \rightarrow \pi^*$ sub-bands in wool samples dyed with cochineal varied from as low as 501 nm to as high as 582 nm for the first sub-band, and ranged from 535 to 604 nm for the second, depending on the dyeing method and mordant [28]. Moreover, other physical factors may also influence the shape of the reflectance spectrum—but not necessarily the position of absorption sub-bands—such as average particle size and overall color density of the paint layer [19, 25, 29]. Considering all these factors, some variation in the exact location of characteristic absorption features is to be expected in the analysis of unknown red pigments in works of art, even when obtained from areas of nominally pure material [17].

Previous efforts have been made to better understand the photophysical and photochemical properties of red lakes using FORS and absorption spectroscopy. Clementi et al. [26] observed differences between the absorption spectra from three different preparations of madder using ultraviolet–visible (UV–Vis) spectroscopy. Attempting to model the heterogeneity of real works of art, Bisulca et al. [19] investigated the effect on the UV–Vis–NIR reflectance spectrum of layering a commercial madder lake and a cochineal lake with vermillion (HgS) and

lead white ($2PbCO_3 \cdot Pb(OH)_2$). Bacci et al. [18] noted the effect of aging on macroscopic color, and consequently on the reflectance spectrum, of organic red lake samples. Golikov and Zharikova [30] examined the impact of varying mordanting salts on the absorption spectra of a cochineal lake associated with collagen using samples from dry films and aqueous solutions.

Because of the challenges intrinsic to the study of these systems, there remains a need to further examine possible correlations between the various chemical syntheses of organic red pigments—particularly those based on madder root and cochineal insects—to the resulting reflectance spectra by FORS. In this work, FORS spectra were collected from well characterized, laboratory-produced madder and cochineal pigments. The results facilitated the ability to:

1. discern correlations between the observed positions of diagnostic absorption features and chemical composition, preparation, and laking substrate of each pigment, as well as the surrounding binder;
2. identify more reliable (i.e., spectroscopically stable) features for the identification of organic red pigments in the reflectance and first derivative transformation spectra despite the variability encountered in the positions of the $n \rightarrow \pi^*$ sub-bands;
3. develop an improved protocol for the identification of madder and cochineal pigments using FORS.

Experimental

Representing the two classes of organic red dyes typically characterized by FORS, madder and cochineal were selected as the focus of this study. Madder and cochineal pigments were prepared from raw materials purchased from Kremer Pigments (#37199 and #36040, respectively) using standardized versions of historical recipes developed by the National Gallery London and published by Kirby et al. [1]. Such standardized recipes consist of procedures where ingredients had their stoichiometric proportions calculated from historical recipes to make these pigments reproducible in the laboratory. Experimental details for each procedure are summarized in Additional file 1: Table S1; synthesis details are found in Kirby et al. [1]. Some recipes traditionally used for the preparation of madder lakes were adapted using cochineal and vice versa for comparative purposes and to create a more extensive reference database. For comparison to the lab-synthesized materials, two cochineal carmines from the Getty Conservation Institute reference collection (GCI DYE15046 and GCI DYE15047) were also included in the study, though the recipes used to make these pigments are not known.

The organic dyestuff composition in each synthesized pigment was verified using HPLC diode-array detection mass spectrometry (HPLC-DAD-MS). For a detailed description of the HPLC methods used and results, see Han et al. [31]. Carminic acid was confirmed to be the primary colorant in all the cochineal samples, and both alizarin and purpurin were identified in the madder samples, as expected based on the synthetic routes employed [31]. The inorganic substrate for each sample was characterized by Fourier Transform Infrared (FTIR) spectroscopy: dry pigment samples were placed on a diamond window, flattened with a metal roller, and analyzed with a Bruker Hyperion 3000 FTIR microscope (transmission mode, $\sim 100 \times 100$ μm aperture, 15× objective, 64 scans at 4 cm^{-1} resolution).

The prepared and characterized pigments were ground and dispersed in four binding media: linseed oil (Kremer Pigments #73054), gum Arabic (Kremer Pigments #63320), egg yolk, and beeswax (Kremer Pigments #62200), and painted out in 1.5×1.5 cm squares on Fredrix® acrylic primed canvas. All paints were prepared following traditional practice as outlined in Additional file 1: Table S2 and described in detail in the literature [32]. Efforts were made to ensure the application of a thin, even layer, with just enough pigmentation to acquire a good quality reflectance spectrum as demonstrated by Bisulca et al. [19]. Such efforts consisted of controlling the thickness of the paint layer by using masking tape (3M 2080EL) as a guide and by applying the paint with a spatula to ensure the surface of each mock up square was level with the tape.

FORS analysis of the painted samples was performed using an ASD FieldSpec 4 Hi-Res fiber optics reflectance spectrometer (Malvern Panalytical). The instrument is equipped with three detectors: a 512 element Si array VNIR detector (350–1000 nm), and two grated index InGaAs photodiode detectors (SWIR 1 [1001–1800 nm] and SWIR 2 [1801–2500 nm]) providing an overall spectral sensitivity from 350 to 2500 nm. Spectral sampling is 1.4 nm between 350–1000 nm, and 2 nm from 1000 to 2500 nm. The spectral resolution is 3 nm at 700 nm and 10 nm at 1400 nm (SWIR 1) and 2100 nm (SWIR 2). The light source is a continuous W-halogen source (ASD PANalytical Fiber Optic Illuminator). All FORS spectra were collected at a fixed geometry: the illumination source was positioned at 45° relative to the sample surface, and the detector was positioned at 90° with respect to the sample surface at a standoff distance of approximately 8 mm. This arrangement yields a spot size at the sample surface approximately 4 mm in diameter. The spectrometer was calibrated against a 99% Spectralon diffuse reflectance standard (Labsphere). Each measurement consists of the average of 64 accumulations, each

with an 8 ms integration time. Five replicate measurements were collected from different points from each sample. All measurements were performed in a dark room to eliminate any contribution from ambient light. FORS spectra were first processed in the ASD ViewSpec Pro 6.2 software, where splice correction was applied, followed by further processing in the Bruker OPUS 7.2 software using log (1/R) and first derivative transformation algorithms. Data analysis was limited to the region 350–1000 nm, given that absorption features above 1000 nm usually relate to the binding medium and are non-diagnostic for the differentiation of anthraquinones.

Results

Representative FORS spectra from cochineal and madder pigments synthesized following seventeenth and eighteenth century historical recipes and painted out in all four binding media are shown in Fig. 1. All spectra present four major characteristic absorption features, visible in each of the traces: two minima between 500 and 600 nm, which will be referred to as $\lambda_{abs,1}$ and $\lambda_{abs,2}$, a shoulder (typically between 470 and 500 nm), $\lambda_{shoulder}$, and the absorption below 400 nm, not used for identification due to consistent noise in that region of the spectrum. As evident in Fig. 1, while the shape of the curve, especially the reflectance maximum between 400 and 500 nm, varies with binding medium, no significant variation in the position of the diagnostic $n \rightarrow \pi^*$ features $\lambda_{abs,1}$ or $\lambda_{abs,2}$ was observed. This is true for all the synthesized pigments in this study. However, it is worth noting that both egg yolk and beeswax contain bands in the visible region of the spectrum at similar wavelengths as these pigments, particularly cochineal, perhaps enhancing diagnostic features, but not interfering with identification. Overall, the data show that the binding medium, due to the lack of prominent spectral features below approximately 800 nm, is not likely to influence the classification of spectra based on features present in the region of interest for identification (400–600 nm). For this reason, except where noted, all spectra subsequently shown are of pigments bound in gum Arabic.

The results by FORS of all the pigments are shown in Fig. 2 and summarized in Table 1, including the positions of spectral features in both reflectance spectra and first derivative transformations. Table 1 also lists substrate types for each pigment, as determined by FTIR. Additional file 2: Figure S1 shows FTIR spectra of all the pigments grouped by substrate type. In contrast to the binding medium, it was found that the synthetic pathway does affect both the position of absorption features, as well as the overall shape of the reflectance spectrum. As will be discussed below, the first derivative features—inflection points located between 500 and 600 nm that relate to $\lambda_{abs,1}$, $\lambda_{abs,2}$, and $\lambda_{shoulder}$ in the reflectance spectrum—provide a more robust measure for the identification of the dyestuff component.

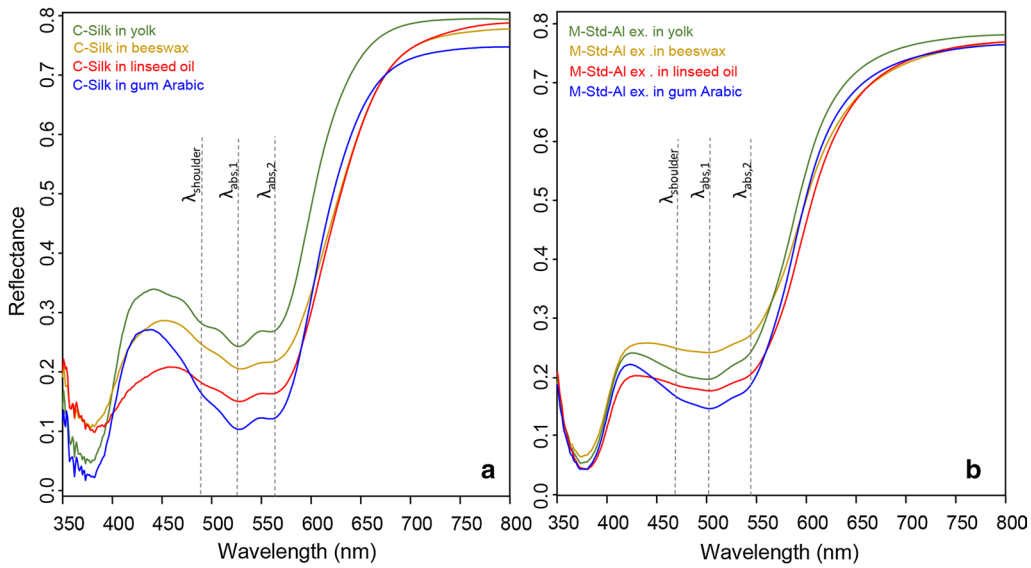

Fig. 1 Representative FORS spectra in four different binders of **a** a cochineal pigment extracted from silk shearings (*C-Silk*), and **b** a madder pigment extracted from the root in an alum solution (*M-Std-Al ex.*). For both pigments, despite some change in the shape of the reflectance spectrum with different binding medium, there is no appreciable change in the position of the $n \rightarrow \pi^*$ absorption features

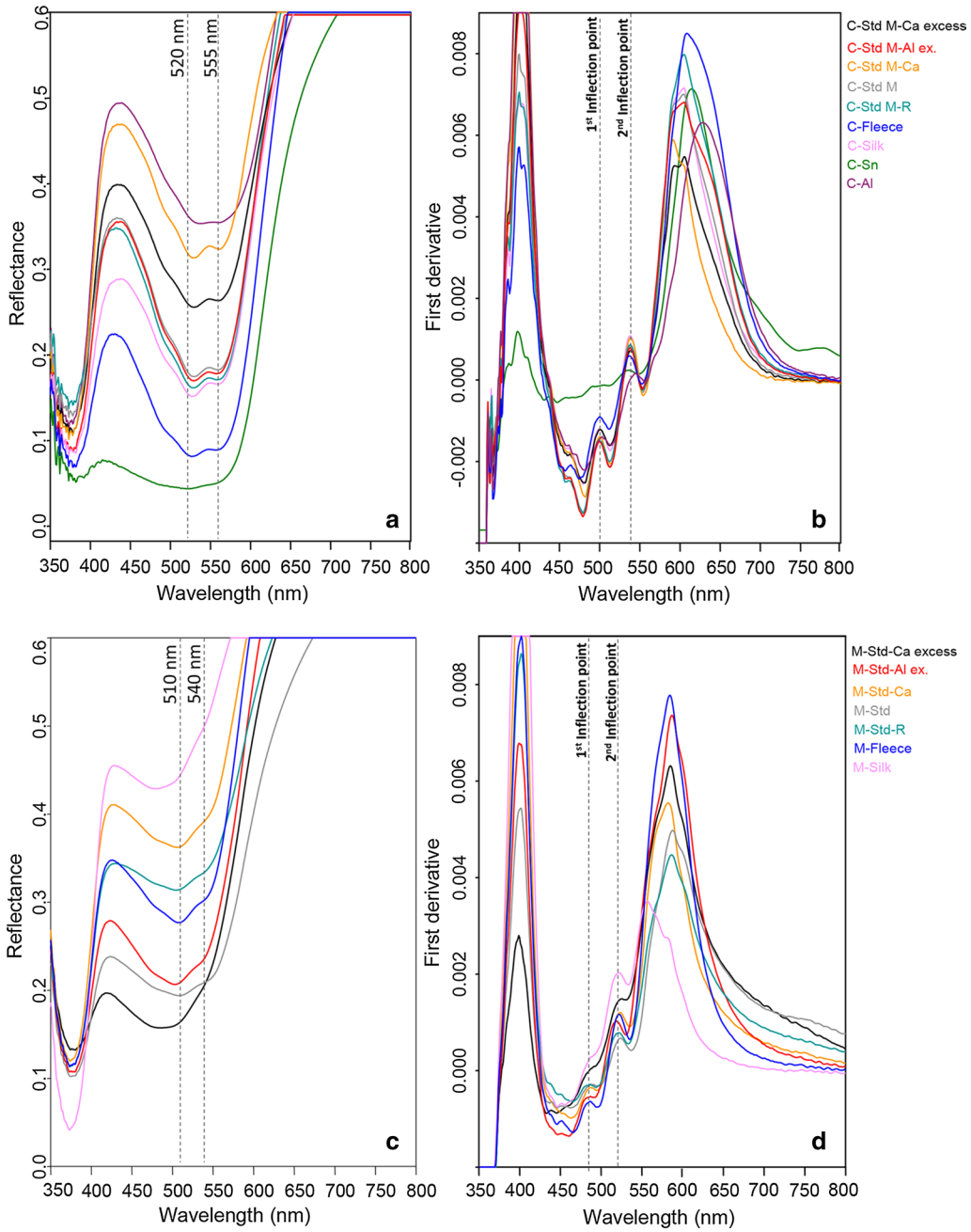

Fig. 2 Reflectance spectrum (left) and first derivative transformation (right) for each synthesized cochineal (**a** and **b**) and madder (**c** and **d**) pigment. Typical literature values for absorption minima are marked to highlight shifts. Relevant inflection points for characterization have also been highlighted. For simplicity, all data presented are of pigments painted in gum Arabic

Discussion

Identification based on first derivative transformations of reflectance spectra

As can be seen in Table 1, the position of the absorption bands assigned to the two $n \rightarrow \pi^*$ transitions ($\lambda_{abs,1}$ and $\lambda_{abs,2}$) show variability across all the samples analyzed. These shifts are non-trivial (on the order of up to almost 20 nm for cochineal and 10 nm for madder—the broad peaks observed for *M-Std-Ca excess* are considered outliers, as will be discussed below), and as such, may impede identification, or lead to misidentification, of the lake pigment. For example, *C-Std M-Ca* (orange trace in Fig. 2a) has a $\lambda_{abs,1}$ at 530 nm, a position intermediate between the literature values usually associated with $\lambda_{abs,1}$ in

Table 1 Position of the characteristic absorption bands in the reflectance spectrum and first derivative inflection points for each synthesized pigment

Pigment	Substrate (determined by FTIR)	FORS features				
		$\lambda_{shoulder}$ (nm)	$\lambda_{abs,1}$ (nm)	$\lambda_{abs,2}$ (nm)	1st inflection point (nm)	2nd inflection point (nm)
C-Std M-R	Alumina, SO_4^{2-}	~495	530 ± 3	557 ± 1	500 ± 0	540 ± 1
C-Std M-Ca excess	$CaCO_3$, alumina	~496	529 ± 2	560 ± 2	500 ± 0	540 ± 3
C-Std M-Ca	$CaCO_3$	~497	530 ± 2	561 ± 1	501 ± 1	540 ± 2
C-Std M	Alumina, SO_4^{2-}	~495	531 ± 2	559 ± 2	500 ± 0	540 ± 2
C-Std M-Al ex.	Alumina, SO_4^{2-}, CO_3^{2-}	~494	530 ± 2	558 ± 2	499 ± 1	539 ± 1
C-Silk	Alumina, SO_4^{2-}, CO_3^{2-}	~496	528 ± 2	559 ± 1	500 ± 1	539 ± 2
C-Fleece	Proteins, alumina, SO_4^{2-}	~497	529 ± 3	558 ± 2	502 ± 3	537 ± 1
C-Sn	Sn salt or complex	~485	520 ± 0	555 ± 1	501 ± 2	535 ± 1
C-Al	Al salt or complex	~493	538 ± 3	574 ± 3	503 ± 3	545 ± 2
DYE15046[a]	Al salt or complex	~489	523 ± 1	562 ± 2	496 ± 1	533 ± 1
DYE15047[a]	Al salt or complex	~489	526 ± 0	562 ± 1	500 ± 1	537 ± 2
M-Std	Alumina, SO_4^{2-}	~481	509 ± 3	~548 (sh)	490 ± 2	524 ± 1
M-Std-R	Alumina, SO_4^{2-}, CO_3^{2-}	~469	500 ± 5	~545 (sh)	~488 (sh)	522 ± 1
M-Std-Al ex.	Alumina, CO_3^{2-}	~475	500 ± 2	~538 (sh)	~486 (sh)	520 ± 2
M-Std-Ca	$CaCO_3$, alumina	~476	506 ± 0	—~545 (sh)	487 ± 0	524 ± 0
M-Std-Ca excess	$CaCO_3$, alumina	nd	480 ± 5 (broad)	~543 (sh)	~487 (sh)	~523 (sh)
M-Silk	Alumina, SO_4^{2-}, CO_3^{2-}	~478 (or maximum, if present)	~502 (sh)	~541 (sh, if present)	~486 (sh)	524 ± 2
M-Fleece	Proteins, alumina, SO_4^{2}	~478	505 ± 3	~542 (sh)	488 ± 1	523 ± 1

The values for $\lambda_{shoulder}$, $\lambda_{abs,1}$, and $\lambda_{abs,2}$ as well as the two first derivative inflection points are averages of the values observed for the same sample across the four binding media examined. Approximate values are presented for features that are present as a shoulder and were visually identified. FTIR spectra taken for substrate characterization of all pigments can be found in Additional file 2: Figure S1

sh shoulder, *nd* not detected

[a] Only painted in gum Arabic for comparison with synthesized pigments

cochineals (520 nm) and madders (540 nm). Similarly, the absorption features in *M-Silk* (pink trace Fig. 2c) are so weak that samples of this material might not be identified as an organic lake pigment at all if no measurable peaks are present.

In contrast, as shown in Fig. 2b and d and summarized in Table 2, the positions of these same absorption features as determined from the inflection points in the first derivative transformation show approximately half as much variability, particularly in the 1st inflection point. For cochineal pigments, the position of the first inflection point was observed between 496 and 503 nm, and the second between 533 and 545 nm. For madder-based pigments, these same features were observed between 486 and 490 nm, and 520 and 524 nm, respectively. Although derivative transformations are routinely used to aid in the interpretation of FORS spectra, it is typically used after interpretation of the reflectance or log (1/R) spectrum. By contrast, when used as a first mean of identification, taken across all pigments studied, the first derivative features provide a means for a more confident discrimination between plant- and animal-based pigments by reflectance spectroscopy. That large shifts in the positions of the absorption minima in the reflectance

Table 2 Range of values measured for the absorption features in the reflectance spectrum and inflection points in the first derivative transformation of cochineal- and madder-based pigments in this study

Features	Cochineal-based pigments	Madder-based pigments
$\lambda_{shoulder}$	~485–497 (Δ ~ 12 nm)	~469–481 (Δ ~ 12 nm)
$\lambda_{abs,1}$	520–538 nm (Δ = 18 nm)	500–509 nm (Δ = 9 nm)
$\lambda_{abs,2}$	555–574 nm (Δ = 19 nm)	~538–548 nm (Δ ~ 10 nm)
1st inflection point	496–503 nm (Δ = 7 nm)	~486–490 nm (Δ ~ 4 nm)
2nd inflection point	533–545 nm (Δ = 12 nm)	520–524 nm (Δ = 4 nm)

Some ranges are presented as approximations because the related features are present as shoulders in the spectra

spectrum give rise to smaller changes in the positions of the inflection points is explained by the fact that the absorption bands from which they arise are relatively weak, and the slope of the reflectance curve between them is small. The first derivative transformations, being a more sensitive measure of changes in absorbance with wavelength, also help in the interpretation of optically dense samples. In all brightly colored layers of paint, the higher the concentration of pigment, the higher the absorption. In FORS, samples are defined as optically dense when only a strong reflectance is visible, showing no apparent diagnostic absorption features in the visible region of the reflectance spectrum. However, in some cases, the first derivative features may still be present in materials that would be classified as optically dense based on their reflectance spectrum. This is illustrated in Fig. 3, which shows the reflectance spectra and first derivative transformation curves of different thicknesses of the carmine pigment *DYE15046*. The diagnostic absorption features are clearly visible in both the reflectance spectra and the first derivative transformations obtained from a thin paint layer, characterized by a high reflectance from the white acrylic priming on the canvas (blue traces, Fig. 3). In contrast, neither the characteristic absorption bands in the reflectance spectrum nor the diagnostic inflection points in the first derivative transformation are visible in spectra obtained from a sample with a much thicker application of paint (green traces, Fig. 3). This sample is truly optically dense. However, in the case of a paint layer with intermediate thickness (red traces, Fig. 3), the first and second inflection points are still observed, even though the $n \rightarrow \pi^*$ absorption features are not readily apparent in the reflectance spectrum, a characteristic that would traditionally classify this sample as optically dense. The first derivative transformation is, therefore, not only a more reliable method for the identification of madder and cochineal pigments, but is also more sensitive, extending the range of pigment densities that are able to be confidently identified. For this reason, the term optically dense should perhaps better be limited to those cases in which both the reflectance spectra and derivative transforms are featureless. It is important to note when analyzing a work of art that, perhaps counter-intuitively, a lighter, thinner layer of paint may be more informative than a richly colored area in terms of obtaining a good quality reflectance spectrum with diagnostic information. This is particularly important for these pigments as their characteristic absorption bands are in the visible region of the spectrum.

Additional information from reflectance spectra of cochineal based pigments

There are three distinguishable important subclasses of cochineal pigments: (i) pink/purple cochineal lakes (*C-Std M-R*, *C-Std M-Ca excess*, *C-Std M-Ca*, *C-Std M*, *C-Std M-Al ex.*, *C-Silk* and *C-Fleece*), in which the coloring

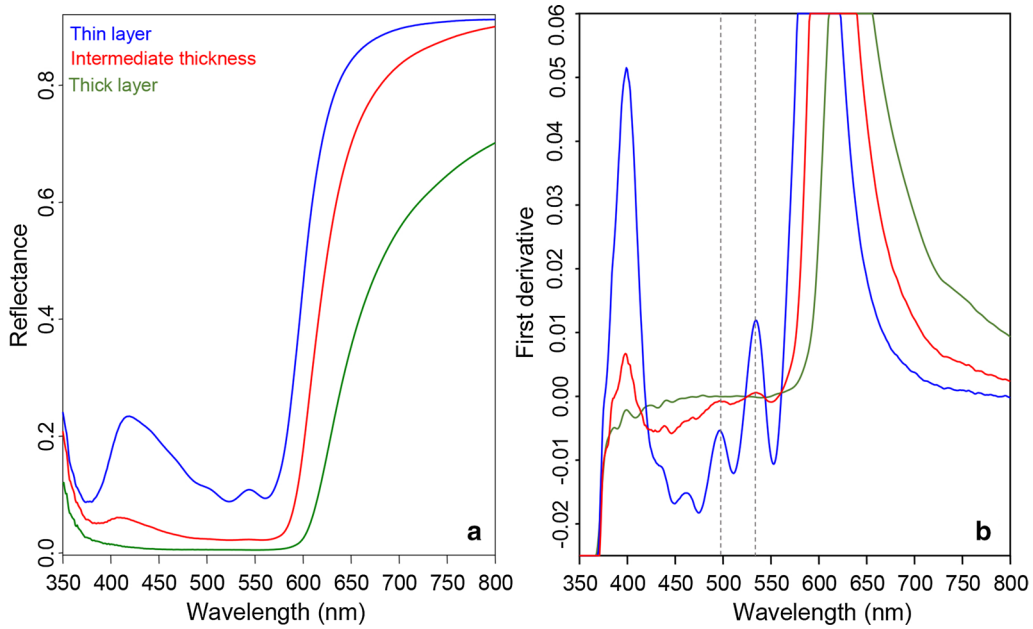

Fig. 3 Reflectance spectra (**a**) and first derivative transformation (**b**) of the cochineal pigment *DYE15046* applied in different paint thicknesses (bound in gum Arabic). Note that the characteristic inflections points (positions marked by dashed lines) are still visible for a sample of intermediate thickness (red traces), although its reflectance spectrum appears featureless

material is adsorbed onto an inorganic substrate, typically some form of hydrated alumina; (ii) scarlet red (an orange-red) tin carmines (*C-Sn*), which are a carminic acid-tin complex, and (iii) crimson red (a bluish-red) aluminum carmines (*C-Al*, *DYE15046*, *DYE15047*) which are a carminic acid-aluminum complex [1, 3, 6]. Notably, of all the cochineal pigments in this study, in all three subclasses, only cochineal tin carmine (*C-Sn*) has absorption bands matching the typical literature values for insect-derived dyes ($\lambda_{abs,1}=520$ nm and $\lambda_{abs,2}=555$ nm) [16, 17], with an additional feature at 485 nm ($\lambda_{shoulder}$). In comparison to *C-Sn*, all other cochineal pigments in this study present some degree of red shift in the position of their features. The cochineal lakes have $\lambda_{shoulder}$ occurring at approximately 494–497 nm, $\lambda_{abs,1}$ at 528–531 nm, and $\lambda_{abs,2}$ at 557–561 nm. The aluminum carmines *DYE15046* and *DYE15047* both have $\lambda_{shoulder}$ at ~489 nm and $\lambda_{abs,1}$ at 523 nm and 526 nm, respectively, only slightly red-shifted from tin carmine values, and $\lambda_{abs,2}$ is at 562 nm for both pigments. However, the aluminum carmine (*C-Al*) synthesized in the laboratory has a more dramatic red shift from *C-Sn*, with $\lambda_{shoulder}$ at 493 nm, $\lambda_{abs,1}$ at 538 nm, and $\lambda_{abs,2}$ at 574 nm. This particular pigment seems to be a special case and will be further addressed below.

Although the pigments used in this study constitute a limited set, they show a promising trend in correlating the synthetic pathway to absorption features in the reflectance spectrum. Figure 4 presents a representative FORS reflectance spectrum from each of the three subclasses of cochineal pigments, together with the unusual *C-Al* synthesized for this work. Swatches of each pigment, showing the range of colors in cochineal-based pigments, are also shown. This variety of hues is due to the chemical properties of carminic acid, the main colorant found in all cochineal pigments and a pH indicator with a critical color change from red to purple occurring between pH 4.8 and pH 6.0 [6, 33, 34]. This color change is associated with the formation of the di-anion of the acid by deprotonation of the hydroxyl in the carboxylic group, followed by deprotonation of one of the hydroxyls attached to the anthraquinone core [33]. Fain et al. [35, 36] correlated these color shifts to displacement of the tautomeric and conformation equilibria of carminic acid and its metal complexes caused by changes in solvent, pH and degree of ionization. Therefore, the shifts observed, albeit small, can be directly related to the final color of each pigment, which, in turn, is intrinsically related to the synthetic pathway of the pigment. All of the cochineal lake pigments in this study [cochineal subclass (i), see *C-Std M*, blue trace in Fig. 4 for a representative example], were synthesized within a narrow temperature range and with an alkali added to the dyestuff solution, either during extraction of the colorant from the insect or dyed

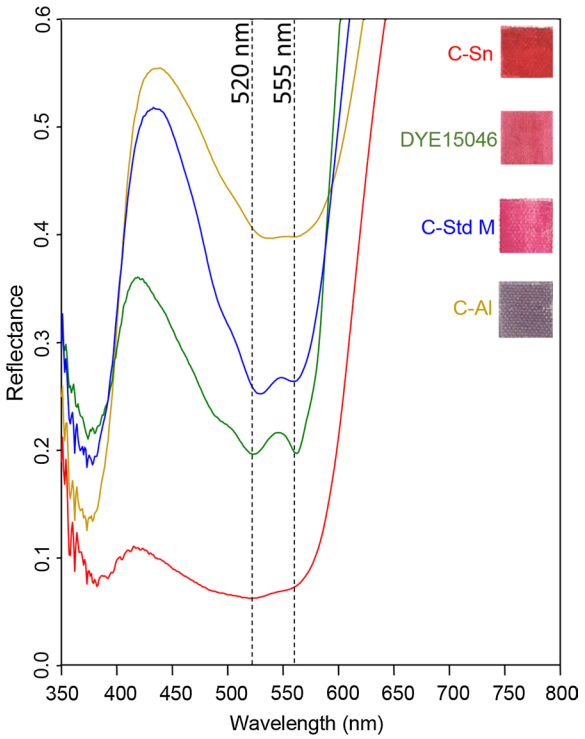

Fig. 4 FORS spectra of the three main types of cochineal based pigments: tin carmine (*C-Sn*), aluminum carmines (*DYE15046* and *C-Al*) and cochineal lake (*C-Std M*). Spectra have been normalized using offset correction (maximum reflectance set to 1.0) and values for the absorption peaks for the tin cochineal carmine (which match typical literature values for cochineal pigments) are marked for comparison

textile or during reaction to precipitate the pigment (see Additional file 1: Table S1). Therefore, the final colors of these pigments are shades of pink and purple, as expected for alkaline solutions containing carminic acid. Because the color of the pigment is related to the pH at which it was produced, for an unknown pigment the precise position of the absorption bands thus can be correlated to the recipe used for its manufacture. From this information, both the laking substrate and most likely period of manufacture may also be inferred. Therefore, if a pigment has $\lambda_{shoulder}$, $\lambda_{abs,1}$ and $\lambda_{abs,2}$ bands between 494–497 nm, 528–531 nm, and 557–561 nm, respectively, it is likely a cochineal lake produced following typical sixteenth and seventeenth century European practice: co-precipitation of the organic dyestuff (traditionally extracted from dyed silk textile shearings) onto an inorganic substrate, most commonly some form of hydrated alumina, with or without the addition of calcium carbonate, by the reaction of alum with an alkali [1, 2, 6].

Analogously, tin carmine *C-Sn* [subclass (ii), red trace in Fig. 4] also has absorption features that can be directly correlated to its mode of manufacture. Tin cochineal

carmines require the addition of tin (IV) chloride to the dyebath to precipitate the pigment, creating a highly acidic solution (pH < 4). Pigments that have little to no substrate and consist mainly of carminic acid as a metal salt or complex (such as the Sn in *C-Sn*) are defined in the literature as 'true' carmine [6]. Recipes of this type, often containing starch as an extender, began appearing in the mid-eighteenth century and were commonly used in the nineteenth century [1]. The tin carmine (*C-Sn*) made in this study has absorption features blue shifted from the aforementioned cochineal lakes, with features located around 485 nm, 520 nm, and 555 nm. Therefore, observation of these features in the reflectance spectrum may indicate the presence of a tin cochineal carmine pigment.

For aluminum carmines [subclass (iii), yellow and green traces in Fig. 4], slightly acidic (pH ≈ 5) [6] conditions are required to promote the precipitation of carminic acid. Most recipes for this type of pigment involve the addition of an acid, like tartaric acid or oxalic acid, together with alum. Such recipes date from the seventeenth century, but became commonplace from the eighteenth century onwards [6]. Both *DYE15046* (green trace in Fig. 4) and *DYE15047* (not shown) fall into this category. The absorption bands of these carmines show $\lambda_{shoulder}$ and $\lambda_{abs,1}$ around 489 nm and 523–526 nm, respectively, i.e., slightly blue shifted from the analogous absorptions for a cochineal lake [subclass (i)]. In contrast, $\lambda_{abs,2}$ for both pigments occurs at 562 nm, slightly red shifted in comparison to a tin carmine [subclass (ii), $\lambda_{abs,2} = 555$ nm]. Detection of these values in an unknown dye, therefore, may be an indication that an aluminum carmine pigment is present. However, caution must be exercised when making this attribution: because aluminum carmines were notoriously difficult to precipitate, sometimes alkali would be added to encourage precipitation, which may cause the pigment to have a higher proportion of hydrated alumina than a 'true' aluminum carmine. Kirby et al. [6] concluded that there is in fact a continuum between a 'true' aluminum carmine (which is a metal complex or salt with little to no substrate) and a cochineal lake (which is the dyestuff precipitated onto an inert substrate). Although careful analysis of FORS spectra may be suggestive of aluminum carmine, a detailed analysis of the substrate by FTIR should be used for confirmation: FTIR spectra of lake pigments will be dominated by features associated with the substrate, whereas the FTIR spectra of carmines, with little or no substrate, will be similar to that of carminic acid, without presenting the characteristic C=O stretch of the carboxylic group at 1720 cm^{-1} [2].

As previously mentioned, *C-Al* (yellow trace in Fig. 4) is not a typical aluminum carmine in terms of color, appearing very dark purple instead of bluish-red (crimson). Consequently, its absorption features are significantly red shifted ($\lambda_{shoulder} \sim 493$ nm, $\lambda_{abs,1} = 538$ nm and $\lambda_{abs,2} = 574$ nm) in comparison to other cochineal pigments examined in this study. The recipe used to make this pigment is one of the earliest carmine recipes, dating from the seventeenth century [6]. Unlike other aluminum carmine recipes, it does not require the addition of any compound other than alum, which has the function of forming the metal complex with carminic acid. Both extraction and the addition of potash alum are carried out at the boiling point of the solution. Previous studies have shown that high temperatures darken carminic acid and can be a major factor in determining the final color of the cochineal based pigment, frequently facilitating the production of purple shades [6, 34]. This likely explains why this particular pigment, despite being an aluminum carmine as confirmed by FTIR, is dark purple and consequently has absorption features shifted to longer wavelengths, even without the addition of an alkali during manufacture. Judging by its color, *C-Al* seems more closely related to what is described in the literature as 'burnt carmine' [34]. Therefore, the existence of pigments of this type must be considered when making the attribution for aluminum carmines by FORS.

Additional information from reflectance spectra of madder based pigments

As with cochineal-based pigments, reflectance spectra of madder pigments also show considerable variability (see Table 1 and Fig. 2c). Three absorption features are distinguishable in the spectra from the pigments in this study, although $\lambda_{abs,2}$ is sometimes only detectable as a shoulder. Typical values of the absorption features range from approximately 469 to 481 for $\lambda_{shoulder}$, 500 nm to 509 nm for $\lambda_{abs,1}$ (not included in this range is the value for *M-Std-Ca excess*, which appears as a broad band centered around 480 nm, and appears to be an outlier, as will be discussed below) and approximately 538 nm to 548 nm for $\lambda_{abs,2}$. Previous studies have shown that the absorption behavior of alizarin and purpurin in solution changes with pH, suggesting a link between absorption and pH (and therefore preparation) [37, 38]. However, this effect is not as easily observed in madder as it was for cochineal due to the complex mixture of colorants present in lakes derived from natural madder root. While alizarin and purpurin are usually cited as the main dyestuffs, one author has listed up to 26 different anthraquinone derivatives in different species of madder [38]. The proportion of each colorant in the final pigment is largely dictated not only by the species of madder used, but also by the recipe used for its manufacture, which ultimately defines its physical and chemical properties [3, 4]. Hence, although it is possible to specifically identify a madder pigment (as distinct from a cochineal pigment) from its

first derivative features, it may not be possible to infer additional information related to the recipe and date of manufacture solely from its reflectance spectrum.

One piece of additional information may be extracted from madder reflectance spectra: the presence of calcium carbonate extenders. Two calcium-containing madder lakes were synthesized in this study: *M-Std-Ca* and *M-Std-Ca excess*. In both cases, calcium carbonate was used to precipitate the pigment, but whereas a stoichiometric amount of alkali was added to neutralize the solution and promote precipitation in *M-Std-Ca*, excess $CaCO_3$ was added to *M-Std-Ca excess* to act as an extender as well as to initiate precipitation. The presence of excess $CaCO_3$ had a significant impact on the absorption spectrum. As can be seen in Fig. 2c and Table 1, *M-Std-Ca excess* (black trace in Fig. 2c) has only one broad absorption band around 480 nm with a shoulder at approximately 543 nm, whereas *M-Std-Ca* (orange trace in Fig. 2c) clearly shows all three absorption features typically observed in madder pigments. Such broadening of the overall absorption region thus may be evidence of the presence of excess calcium carbonate in the pigment, which may increase the effect of physical factors—such as the average particle size and the location of the dyestuff in the paint layer—on the shape of the spectrum. Interestingly, the same effect was not observed for cochineal based pigments. It may be that larger quantities of calcium carbonate are needed to produce the same effect in cochineal-based pigments, though assessing that trend was not within the scope of this paper.

Decision tree for the specific identification of madder and cochineal pigments

The results discussed above have been summarized in a decision tree to facilitate the identification of madder and cochineal-based pigments in works of art using FORS (see Fig. 5). It is important to note that, to avoid misidentification, before the protocol is applied there must be some indication of the presence of an organic red pigment. Such indications may include the observation of characteristic fluorescence in the UV, lack of evidence from XRF analysis for an inorganic red pigment, or FORS spectra presenting the characteristic shape of an organic red colorant, as discussed in previous sections.

Since it is common practice to examine FORS data as apparent absorbance (log (1/R)) to enhance weak absorption features [17, 26], both reflectance and apparent absorbance spectra are presented in Fig. 5 for convenience. The protocol outlined in the decision tree has been validated by the examination of FORS data collected from several works of art, two of which are presented below. The protocol uses the first derivative transformation for the initial identification of the pigment, followed by examination of shifts in the $n \rightarrow \pi^*$ features in the reflectance spectra to add specificity to the identification, particularly in the case of cochineal. The ranges presented in the decision tree are slightly extended with respect to the values found in this study to take into consideration the spectral resolution of the equipment and standard deviation of the measurements.

Validation case study #1: Model Resting—Henri de Toulouse-Lautrec (1889)

A FORS spectrum was acquired from a pink area on the lap of the figure in Henri de Toulouse-Lautrec's *Model Resting*, 1889 (red traces in Fig. 6a). Following the decision tree protocol, the first derivative transformation is first examined, and it can be seen that there are diagnostic inflection points, in this case occurring at 487 and 524 nm, which fall into the ranges suggesting the presence of a madder pigment. Next, examining the reflectance spectrum (presented here as apparent absorbance), it can be seen that it presents typical features of an organic red pigment: the absorption sub-bands located between 500 and 600 nm, the local reflectance maximum in the blue region, and a gradual shallow increase in reflectance throughout the red region of the visible spectrum. Absorption features are located at 517 nm and 549 nm, and no shoulder feature below 500 nm is observed. These values fall outside of the ranges observed in Table 2, so if only the reflectance spectrum was examined it would be difficult to tell whether this is a plant or animal based organic red pigment. However, as discussed, the first derivative transformation is a more robust means of making the initial cochineal/madder distinction than the reflectance/apparent absorbance curves. Comparing spectra from a standard madder pigment (*M-Std*, black traces in Fig. 6a), with those obtained from the painting, it seems that while the apparent absorbance curves appear to be quite different, the characteristic inflection points in the first derivative transformations occur at approximately the same position. The differences observed in the apparent absorbance curves are due to the complex nature of the sample, although salient features relating to the organic red pigment are still present. Therefore, when the first derivative transformation is applied, diagnostic features are enhanced, enabling identification. Given the date of the painting (1889), synthetic alizarin could have also been a possibility, since it would have been in production by that time [38]. Therefore it is important to consider this possibility in artworks from the late nineteenth century onwards. HPLC analysis of a sample obtained from the same area [39] found the presence of both alizarin and purpurin, confirming that this was, indeed, a madder pigment.

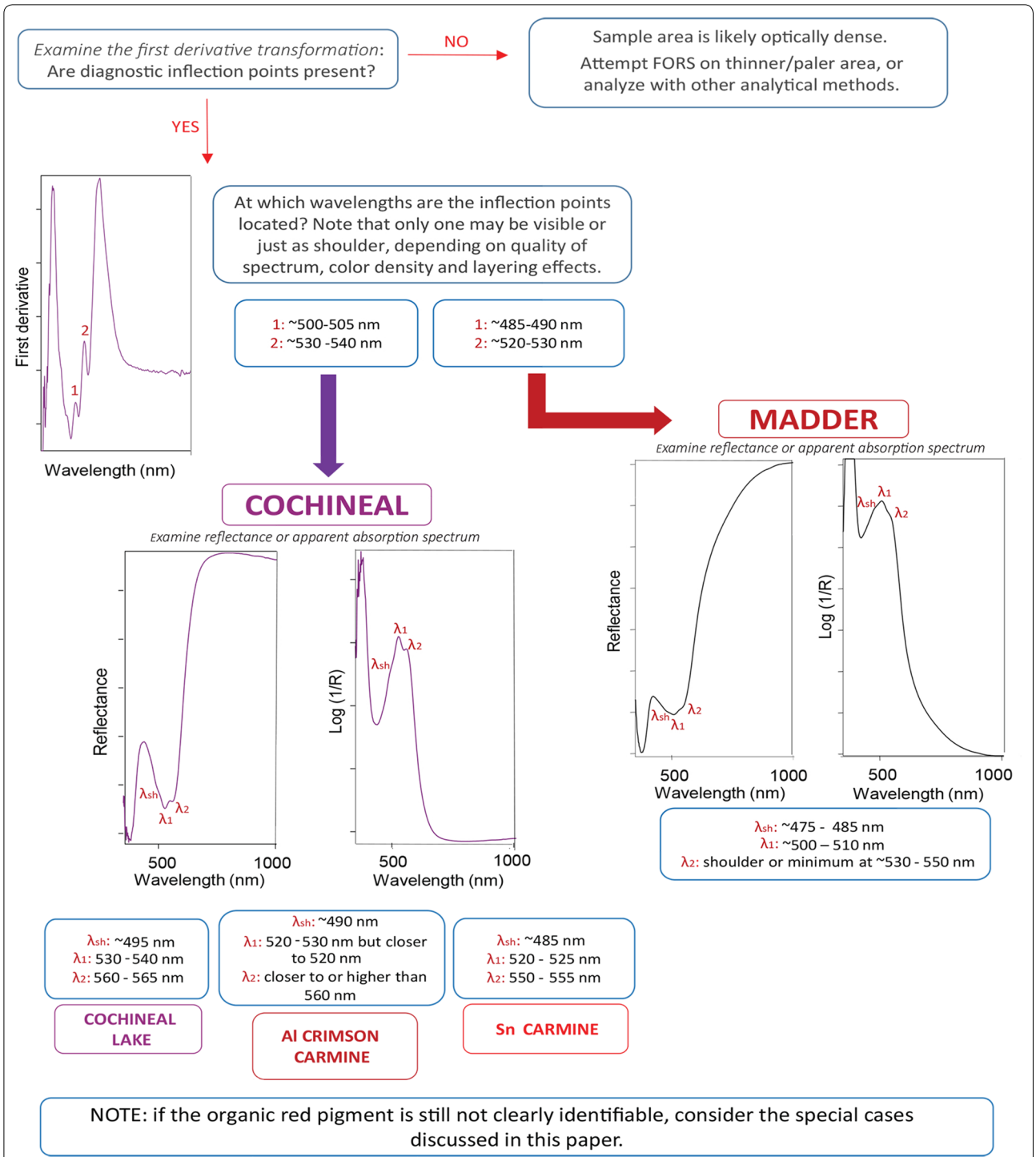

Fig. 5 Decision tree for the identification of madder- and cochineal-based pigments in works of art. For general identification purposes, the ranges shown here have been slightly extended from those measured in this study to allow for variability in individual measurements due to differences in instrumental setup and performance

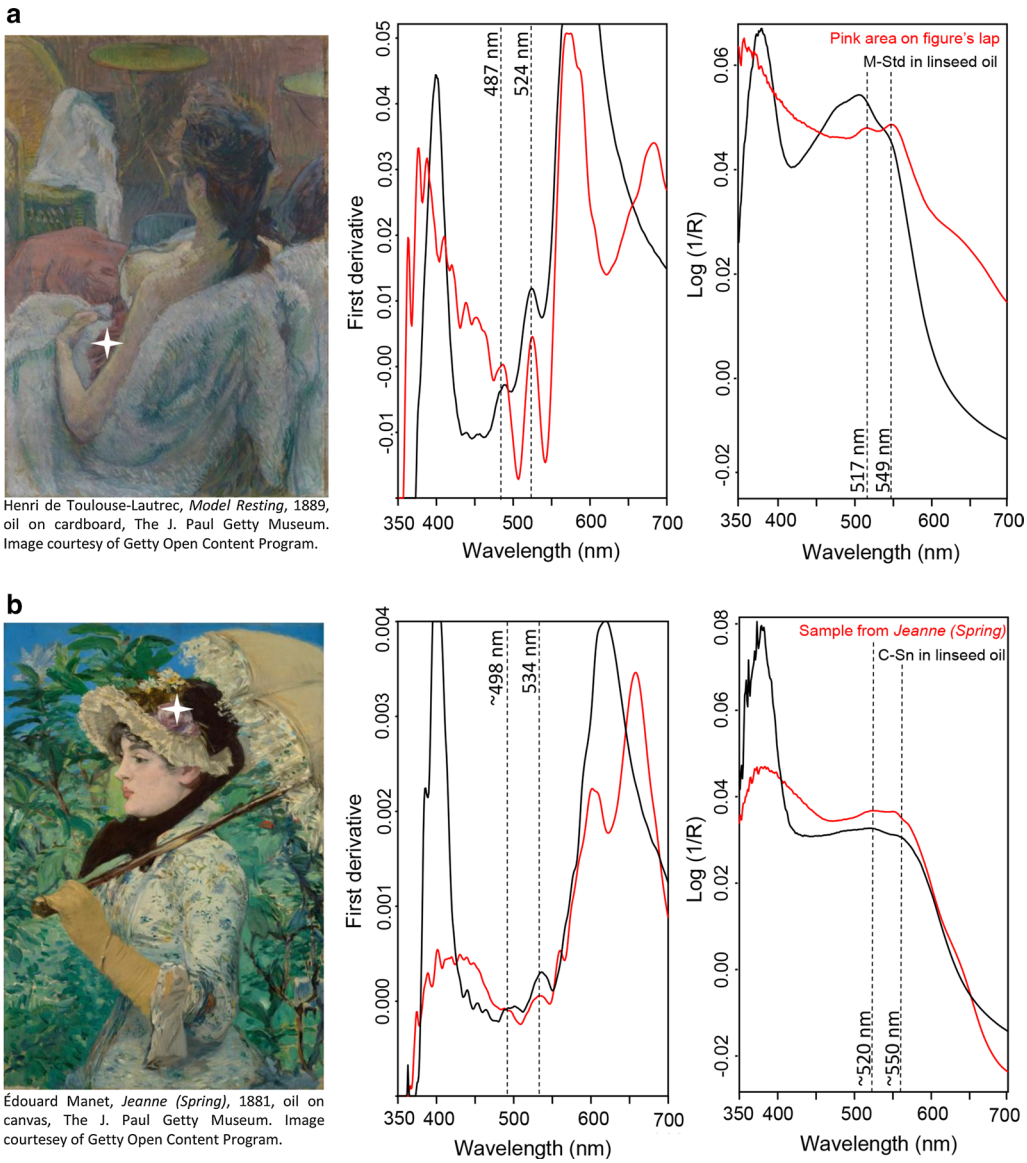

Fig. 6 First derivative (left) and apparent absorbance spectrum (right) of **a** a pink area on lap of figure on Henri de Toulouse-Lautrec's *Model Resting* (1889, oil on cardboard, The J. Paul Getty Museum, 84.PC.39) (red curve) compared against a standard madder lake (*M-Std*) in linseed oil (black curve); and **b** a pink/red flower on the bonnet of Édouard Manet's *Jeanne* (1881, oil on canvas, The J. Paul Getty Museum, 2014.62) (red curve) compared against a tin cochineal carmine made in the laboratory (black curve). Sampled areas are marked with a white cross

Validation case study #2: Jeanne (Spring)—Édouard Manet (1881)

Another validation test of the decision tree was performed using data from Manet's *Jeanne* (*Spring*), 1881; the FORS spectrum and its first derivative transformation of a red area are shown in Fig. 6b (red traces). The first derivative transformation has an inflection point at 534 nm and there is a shoulder at approximately 498 nm. As outlined in Fig. 5 and Table 2, together, these features are consistent with those observed for cochineal-based pigments. Next, examining the apparent absorbance (log (1/R)) spectrum, it can be seen that although the absorption bands are not clearly defined, weak features are present at approximately 520 and 550 nm, suggesting the presence of a tin cochineal carmine pigment, though the expected shoulder that usually appears at approximately 485 nm was not detected. The presence of Sn was confirmed by SEM–EDS analysis of a cross section containing the analyzed pigment (not shown). Visual analysis of the cross section also suggests that starch, a typical

extender for tin carmines [6], was present in the paint layer. HPLC analysis confirmed the identity of the colorant as carminic acid, but interestingly, also found traces of madder. The presence of both cochineal and madder may have contributed to the fact that the peaks were less well defined than typically observed for pure components, both in the reflectance spectrum [40] as well as the first derivative transformation. Nonetheless, FORS analysis successfully identified the primary colorant in the paint layer. However, it is worth noting that additional analysis on a removed sample by HPLC was still required to identify additional colorants present in trace quantities, highlighting the fact that FORS cannot typically be considered an exhaustive analytical technique.

Conclusions

In the analysis of FORS spectra of organic red pigments, the traditionally-used absorption features can present shifts that are great enough to hinder even a broad classification of plant versus animal origin. This work has shown that shifts in the positions of the inflection points in the first derivative transformation are smaller in comparison to the related absorption features, and thus provide a more robust diagnostic for confidently discriminating between madder and cochineal pigments. However, the reflectance spectra also contain important information. Although the set of pigments studied here is limited, a promising trend was identified. Specifically, small shifts in features in the reflectance spectra of cochineal-based pigments were shown to be linked to the recipes used for their synthesis. The pH of the solution used for extraction of the dyestuff from the raw material or for the reaction to precipitate the pigment is one of the major determinants of the final pigment color, and thus is reflected in the FORS spectrum. Once identified as a cochineal, the position of the absorption bands can help further discriminate whether it is a cochineal lake, an aluminum carmine, or a tin carmine. Unfortunately, the complex chemical composition of madder pigments, with more than ten different colorants that may all act synergistically in influencing the position of absorption bands, prevents as detailed an analysis through FORS data alone, though some indication of the presence of calcium carbonate in the recipe may be discernible.

From the data collected in this study, a decision tree to help researchers identify cochineal and madder pigments on works of art using FORS was created. The protocol was successfully tested on several case studies, two of which were presented here. These consisted of two nineteenth century paintings for which other confirmatory data was available. The protocol correctly identified the primary colorant in each case. In one case, madder was correctly detected, and in the second case cochineal (specifically, a tin carmine) was correctly suggested to be the primary colorant by FORS, although trace amounts of madder were also present, and only identified by HPLC. Therefore, it is important to note that even though a particular organic dyestuff may not be detectable by FORS, it may still be present. It is also important to note that this study was carried out on a limited set of pure unaged samples prepared in the laboratory. Colorants found in works of art may differ from those examined here due to the presence of mixtures and different material layers that may ultimately affect the reflectance spectrum. Therefore, it is necessary to proceed with caution when analyzing artworks and be aware of synergetic effects other materials may have on the resulting FORS spectra. When in doubt, other techniques such as HPLC should be used to confirm the identification. Further investigation is needed to more fully assess how layering, mixing, and ageing affect the position of diagnostic absorption features for madder and cochineal pigments in their reflectance spectra and first derivative transformations. Moreover, similar systematic research into other related organic red dyestuffs such as kermes, lac (both anthraquinones with similar spectral features), and synthetic alizarin is needed to build a more complete decision tree for the unambiguous identification of organic red pigments by FORS.

Supplementary information

Supplementary information accompanies this paper at https://doi.org/10.1186/s40494-019-0335-1.

Additional file 1: Table S1. Summary of the recipes used to prepare the madder and cochineal pigments. In most cases, adaption of recipes consists in adapting the temperature of reaction to the dyestuff source (70–80 °C for madder and 40–50 °C for cochineal). Ca-containing substrates were made using standard madder and cochineal recipes but substituting the alkali used for $CaCO_3$. **Table S2.** Summary of procedures used to make paints using linseed oil, gum Arabic, yolk and beeswax. No additives were added to any of the paints to avoid interference with analysis and to build a reference database of mixtures containing just the binder and the pigment.

Additional file 2: Figure S1. FTIR spectra for substrate characterization of all synthesized pigments, including the pigments *DYE15046* and *DYE15047* from the GCI reference collection. All spectra have been vector normalized for comparison. Reference substrates have been synthesized without the dyestuff using recipes described in Table S.1. For simplicity, only characteristic bands of the references are marked for comparison. (A) Pigments with alumina substrates with varying amounts of carbonate (amorphous hydrated form) and sulfate (light hydrated form); (B) Pigments with calcium carbonate as the main substrate component; (C) Pigments containing wool protein in the alumina substrate; (D) Carmine pigments with little or no substrate similar to pure carminic acid except for the C=O stretch band at 1720 cm^{-1}, which is absent [2, 41, 42].

Acknowledgements

The authors would like thank Jo Kirby for her invaluable and tireless help in adapting recipes and understanding the ramifications of synthetic variations. At the Getty Conservation Institute, we thank Herant Khanjian for offering his expert knowledge to ensure the best quality FTIR spectra were collected

and Jing Han for conducting HPLC analysis on all pigments. We also thank the paintings curatorial and conservation departments at the J. Paul Getty Museum for providing works of art for analysis.

Authors' contributions

BF synthesized all pigments, collected and interpreted data. CSP and DM presented the question that originated the research and provided critical feedback shaping the experiments. MG and KT supervised BF during the project. CSP carried out analysis of samples from *Manet's Jeanne* (*Spring*). BF took the lead in writing the manuscript, but all authors contributed to editing and shaping the final version. All authors read and approved the final manuscript.

Funding

Funding was provided by the Getty Graduate Internship provided by The J. Paul Getty Trust and hosted by the Department of Science at the Getty Conservation Institute.

Availability of data and materials

The datasets used and/or analyzed during the current study are available from the corresponding author on reasonable request.

Competing interests

The authors declare that they have no competing interests.

Author details

[1] Getty Conservation Institute, 1200 Getty Center Drive, Suite 700, Los Angeles, CA 90049, USA. [2] Present Address: University of Copenhagen, Øster Farimagsgade 5, 1353 Copenhagen K, Denmark.

Received: 23 July 2019 Accepted: 30 October 2019
Published online: 08 November 2019

References

1. Kirby J, van Bommel M, Verhecken A, Spring M, Vanden Berghe I, Stege H, Richter M. Natural colorants for dyeing and lake pigments: practical recipes and their historical sources. London: Archetype Publications; 2014.
2. Kirby J, Spring M, Higgitt C. The technology of red lake pigment manufacture: study of the dyestuff substrate. Natl Gall Tech Bull. 2005;26:71–87.
3. Hofenk de Graaff JH, Roelofs WGT, van Bommel MR. The colourful past : origins, chemistry and identification of natural dyestuffs. London: Archetype Publications ; Abegg-Stiftung; 2004.
4. Daniels V, Devièse T, Hacke M, Higgitt C. Technological insights into madder pigment production in antiquity. Br Museum Tech Res Bull. 2014;8:13–28.
5. Rodríguez ES. Proof positive: the science of finding cochineal. In: Padilla C, Anderson B, editors. A red like no other: how cochineal colored the world. New York: Skira Rizzoli; 2015. p. 100–3.
6. Kirby J, Spring M, Higgitt C. The technology of eighteenth- and nineteenth-century red lake pigments. Natl Gall Tech Bull. 2007;2017(28):69–95.
7. Cuoco G, Mathe C, Archier P, Vieillescazes C. Characterization of madder and garancine in historic French red materials by liquid chromatography-photodiode array detection. J Cult Herit. 2011;12(1):98–104. https://doi.org/10.1016/j.culher.2010.05.005.
8. Kirby J, White R. The identification of red lake pigment dyestuffs and a discussion of their use. Natl Gall Tech Bull. 1996;17:56–80.
9. Wouters J, Grzywacz CM, Claro A. A comparative investigation of hydrolysis methods to analyze natural organic dyes by HPLC-PDA. Stud Conserv. 2011;2:231–50.
10. Berrie BH. An improved method for identifying red lakes on art and historical artifacts. Proc Natl Acad Sci USA. 2009;106:15095–6.
11. Idone A, Aceto M, Diana E, Appolonia L, Gulmini M. Surface-enhanced Raman scattering for the analysis of red lake pigments in painting layers mounted in cross sections. J Raman Spectrosc. 2014;45:1127–32.
12. Whitney AV, Van Duyne RP, Casadio F. An innovative surface-enhanced Raman spectroscopy (SERS) method for the identification of six historical red lakes and dyestuffs. J Phys Org Chem. 2006;37:993–1002.
13. Pozzi F, van den Berg J, Fiedley I, Casadio F. A systematic analysis of red lake pigments in French impressionist and post-impressionist paintings by surface-enhanced Raman spectroscopy (SERS). J Raman Spectrosc. 2014;45:1119–26.
14. Claro A, Melo MJ, Schaefer S, Seixas de Melo JS, Pina F, van den Berg KJ, Burnstock A. The use of microspectrofluorimetry for the characterization of lake pigments. Talanta. 2008;74:922–9.
15. Nabais P, Melo MJ, Lopes JA, Vitorino T, Neves A, Castro R. Microspectrofluorimetry and chemometrics for the identification of medieval lake pigments. Herit Sci. 2018. https://doi.org/10.1186/s40494-018-0178-1.
16. Delaney JK, Zeibel JG, Thoury M, Littleton ROY, Palmer M, Morales KM, Rene E, Hoenigswald ANN. Visible and infrared imaging spectroscopy of Picasso' s Harlequin Musician: mapping and Identification of artist materials in situ. Appl Spectrosc. 2010;64(6):584–94.
17. Aceto M, Agostino A, Fenoglio G, Idone A, Gulmini M, Picollo M, Ricciardi P, Delaney JK. Characterisation of colourants on illuminated manuscripts by portable fibre optic UV-visible-NIR reflectance spectrophotometry. Anal Methods. 2014;6(5):1488–500. https://doi.org/10.1039/C3AY41904E.
18. Bacci M, Orlando A, Picollo M, Radicati B, Laterna G. Colour analysis of historical red lakes using non-destructive reflectance spectroscopy. In: Compatible materials for the protection of cultural heritage PACT58. Technical Chamber of Greece; 2000. p. 21–35.
19. Bisulca C, Picollo M, Bacci M, Kunzelman D. Uv-Vis-Nir reflectance spectroscopy of red lakes in paintings. In: 9th international conference NDT Art. 2008; p. 1–8.
20. Reta MR, Cattana R, Anunziata JD, Silver JJ. Solvatochromism of anthraquinone and symmetrical dihydroxy derivatives. Local interactions. Spectrochim Acta. 1993;49A(7):903–12.
21. Langdon-Jones EE, Pope SJA. The coordination chemistry of substituted anthraquinones: developments and applications. Coord Chem Rev. 2014;269:32–53.
22. Hartman FH. Light absorption of organic colorants: theoretical treatment and empirical rules. Berlin: Springer; 1980.
23. Hoffmann R, Swenson JR. The interaction of nonbonding orbital in carbonyls. Helv Chim Acta. 1970;53(277):2331–8.
24. Yoshida Z, Taicabayashi F. Electronic spectra of mono-substituted anthraquinones and solvent effects. Tetrahedron. 1968;24:913–43.
25. Bacci M. UV-Vis-NIR, FTIR, and FORS Spectroscopies. In: Ciliberto E, Spoto G, editors. Modern analytical methods in art and archaeology. Hoboken: Wiley; 2000. p. 321–57.
26. Clementi C, Doherty B, Gentili PL, Miliani C, Romani A, Brunetti BG, Sgamellotti A. Vibrational and electronic properties of painting lakes. Appl Phys A. 2008;92:25–33.
27. Vitorino T, Casini A, Cucci C, Melo MJ, Picollo M, Stefani L. Hyper-spectral acquisition on historically accurate reconstructions of red organic lakes. In: Elmoataz A., Lezoray O., Nouboud F. MD, editor. Image and signal processing ICISP 2014 lecture notes in computer science. Berlin: Springer; 2014. p. 257–64.
28. Morales KM, Berrie BH. A note on characterization of the cochineal dyestuff on wool using microspectrophotometry. e-Preservation Sci. 2015;12:8–14.
29. Kortüm G. Reflectance spectroscopy: principles, methods and applications. New York: Springer; 1969.
30. Golikov V, Zharikova Z. A study of model carminic acid lakes prepared using cochineal, collagen and different mordant salts. In: Kirby J, editor. Dyes in history and archaeology, vol. 21. London: Archetype; 2008. p. 134–47.
31. Han J, Fonseca B, Ganio M, MacLennan D, Schilling MR. Normalized peak area distributions with HPLC-DAD-MS as a tool for differentiating madder and cochineal lakes in easel paintings. In: American Institute of conservation's 47th annual meeting. New England; 2019.
32. Gottsegen MD. The painter's handbook: a complete reference. New York: Watson-Guptill Publications; 2006.
33. Favaro G, Miliani C, Romani A, Vagnini M. Role of protolytic interactions in photo-aging processes of carminic acid and carminic lake in solution and painted layers. R Soc Chem. 2002;2:192–7.
34. Schweppe H, Roosen-Runge H. Carmine—cochineal carmine and kermes carmine. In: Feller RL, editor. Artitsts' pigments: a handbook of their history and characteristics, vol. 1. London: Archetype Publications; 1986. p. 255–83.
35. Fain VY, Zaitsev BE, Ryabov MA. Tautomerism and ionization of carminic acid. Russ J Gen Chem. 2007;77(10):1769–74.

36. Fain VY, Zaitsev BE, Ryabov MA. Tautomerism of metal complexes with carminic acid. Russ J Coord Chem. 2008;34(4):310–4.
37. Miliani C, Romani A, Favaro G. Acidichromic effects in 1,2-di- and 1,2,4-trihydroxyanthraquinones. A spectrophotometric and fluorimetric study. J Phys Org Chem. 2000;13:141–50.
38. Schweppe H, Winter J. Madder and Alizarin. In: FitzHugh EW, editor. Artitsts' pigments: a handbook of their history and characteristics, vol. 3. New York: Oxford University Press; 1997. p. 109–42.
39. Han J. GCI science materials characterization laboratory internal report: organic reds in model resting—Toulouse-Lautrec. Los Angeles; 2018.
40. Ormond D, Patterson CS. The Making of a Parisienne: Manet's Methods and Materials. In: Allan S, Beeny EA, Groom G, editors. Manet and modern beauty: the artist's last years. Los Angeles: J Paul Getty Museum; 2019. p. 147–59.
41. Silverstein RM, Kiemle DJ, Webster FX, Bryce DL. Spectrometric identification of organic compounds. New York: Wiley; 2015.
42. Nyquist RA, Leugers MA, Putzig CL. Infrared and Raman spectral atlas of inorganic compounds and organic salts : Raman spectra. San Diego: Academic Press; 1997.

Publisher's Note